JOURNAL OF GEOPHYSICAL RESEARCH, VOL. 115, C07012, doi:10.1029/2009JC005620, 2010

High-frequency forcing and subtidal response of the Hudson River plume

Elias J. Hunter,[1] Robert J. Chant,[1] John L. Wilkin,[1] and Josh Kohut[1]

Received 6 July 2009; revised 5 February 2010; accepted 8 March 2010; published 21 July 2010.

[1] The Lagrangian Transport and Transformation Experiments (LaTTE) document the physical, biological, and chemical evolution of the Hudson River plume during the spring seasons of 2004, 2005, and 2006. While plume variability due to river discharge, subinertial frequency variability in winds, and ambient shelf circulation are important, the observations show that the plume reacts directly to higher-frequency forcing as well. Mooring records during 2005 and 2006 show that fortnightly variability in tidal mixing is manifested as fortnightly changes in plume stratification. Diurnal variability related to forcing by the sea-land breeze system (SLBS) is apparent in the Hudson River plume during the 2005 experiment. The SLBS, while episodic, accounts for ~15% of the kinetic energy in surface currents in the New York Bight apex during the summer months with individual SLBS events providing up to 50% of the total kinetic energy. Simulations of the plume, using the Regional Ocean Modeling System (ROMS), demonstrate there is a subtidal response to high-frequency forcing. Spring-neap variability in tidal mixing modifies the estuary outflow Rossby and Froude numbers, resulting in increased transport (80% of river discharge) in the New Jersey coastal current during spring tides with lower transport (60% of river discharge) during neap tides. SLBS variability results in greater storage of river discharge water in the recirculating bulge region and increases the net transport of freshwater along the Long Island coast while significantly reducing freshwater supplied to the New Jersey coastal current to as little as 30% of the total river discharge.

Citation: Hunter, E. J., R. J. Chant, J. L. Wilkin, and J. Kohut (2010), High-frequency forcing and subtidal response of the Hudson River plume, *J. Geophys. Res.*, *115*, C07012, doi:10.1029/2009JC005620.

1. Introduction

[2] River discharge to the inner continental shelf influences variability across a range of time scales in many coastal ocean regions worldwide. The large freshwater flux associated with rivers (particularly during the spring freshet) leads to the development of well-documented hydrographic features such as fronts, jets, and recirculating eddies on the inner shelf [*Castelao et al.*, 2008; *Orton and Jay*, 2005]. In addition, river plumes can play a first-order role in the transport and dispersal of sediment, biota, nutrients, and anthropogenic contamination in the coastal zone. This has implications for coastal biological and chemical processes and is particularly relevant in a highly urbanized estuary such as the Hudson River [*Levinton and Waldman*, 2006].

[3] These buoyant river plumes are often classified according to their dominant dynamical balance and divided into two groups depending on their interaction with the ocean bottom [*Avicola and Huq*, 2002; *Lentz and Helfrich*, 2002; *Yankovsky and Chapman*, 1997]. The "bottom-advected" plume has low-salinity water extending from the surface to the bottom. The plumes momentum drives an offshore buoyancy flux in the bottom Ekman layer that produces a well-defined bottom-attached front that isolates the inshore plume from the offshore waters. The offshore location of this front and the isobath that it resides on is often well predicted by theory [*Chapman and Lentz*, 1994]. The "surface-advected" plume, on the other hand, is a shallow buoyant layer overlaying a more dense background fluid and has little or no direct interaction with the seafloor. For the purposes of this study, we restrict discussion to surface-advected plumes, which typically characterizes the Hudson River plume [*Avicola and Huq*, 2002; *Chant et al.*, 2008; *Yankovsky and Chapman*, 1997].

[4] Numerical modeling studies and laboratory tank experiments demonstrate that the idealized surface-advected plume has two distinct dynamic regions: a coastal gravity current that propagates down shelf (in the Kelvin wave sense) and a recirculating low-salinity "bulge" near the river outflow [*Avicola and Huq*, 2003a, 2003b; *Chao and Boiucourt*, 1986; *Chapman and Lentz*, 1994; *Fong and Geyer*, 2002; *Nof and Pichevin*, 2001]. The cross-shore dynamics of the coastal current are primarily geostropic, while those of the

[1]Institute for Marine and Coastal Sciences, Rutgers, State University of New Jersey, New Brunswick, New Jersey, USA.

0148-0227/10/2009JC005620

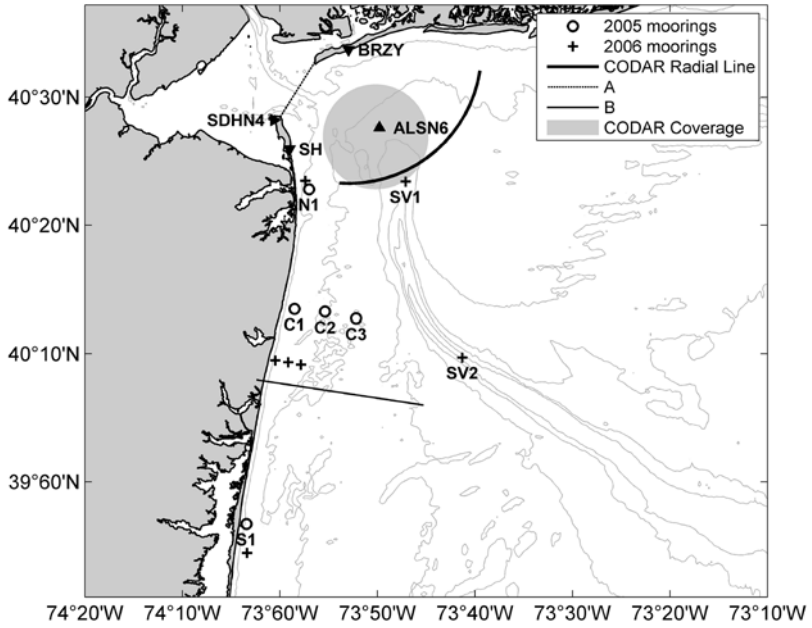

Figure 1. The above map shows the locations of observational data stations in the LaTTE study area. Included are the CODAR installations at Sandy Hook (SH) and Breezy Point (BRZY), NBDC stations at Sandy Hook (SDHN4) and Ambrose Tower (ALSN6), and the mooring locations during LaTTE 2005 and 2006. Also noted are a CODAR radial arc from BRZY and the approximate footprint of CODAR coverage for BRZY and SH. Lines A and B are the locations of cross sections extracted from ROMS simulations.

anticyclonically rotating bulge are weakly cyclostrophic, whereby the cross-stream pressure gradient is balanced by the sum of Coriolis and centrifugal accelerations.

[5] The extensive literature on buoyant river plumes identify, through characteristic length scales and nondimensional numbers, regimes describing plume spatial and temporal variability and highlight the important dynamical balances of the river outflow. *Garvine* [1995] classifies buoyant plumes according to a Kelvin number, which is the ratio of the cross-shore length scale of the coastal current to the baroclinic Rossby radius. Coastal currents with small Kelvin number are dominated by nonlinear momentum advection terms with little contribution from the Coriolis effect, while large Kelvin number flows are associated with weak advection and relatively strong Coriolis terms. *Yankovsky and Chapman* [1997] derived length scales (plume width and depth) from the basic dynamics of surface-advected and bottom-advected plumes and further framed these scales as Froude (F_i), Rossby (R_o), and Rossby (S) numbers, defined as

$$F_i = v_i/(g_i' h_o)^{1/2}, \tag{1}$$

$$R_o = v_i/fL, \tag{2}$$

$$S = R_o/F_i, \tag{3}$$

where v_i is the mean outflow velocity, g_i' is reduced gravity ($g_i' = g\Delta\rho/\rho_o$), f is the Coriolis parameter, and L is the width of the outflow.

[6] The resulting parameter space is useful in determining whether a plume is surface or bottom advected based on inflow properties and bottom slope. *Yankovsky and Chapman* [1997] applied the scaling framework to a series of numerical model runs and observational data, noting that the Hudson River plume is surface advected, as did *Avicola and Huq* [2002].

[7] The recirculating bulge region of a surface-advected plume is documented in many laboratory experiments and numerical simulations of buoyant river plumes [*Avicola and Huq*, 2003a, 2003b; *Fong and Geyer*, 2002; *Horner-Devine et al.*, 2006; *Nof and Pichevin*, 2001; *Yankovsky and Chapman*, 1997; *Garvine*, 2001]. While the underlying dynamics that govern the rate of bulge growth remains elusive, both *Avicola and Huq* [2003a, 2003b] and *Horner-Devine et al.* [2006] suggest that outflow geometry plays a central role in bulge formation. There is, however, little observational evidence. While the recirculating bulge region of a river plume is more difficult to observe fully in nature, there is ample evidence of the feature in the Hudson River plume [*Chant et al.*, 2008], the Columbia River plume [*Horner-Devine*, 2008; *Hickey et al.*, 1998] and the Niagara River plume [*Masse and Murthy*, 1990, 1992; *Horner-Devine et al.*, 2008]. The Hudson River mouth has a particularly complicated coastal geometry (Figure 1), which has been shown should favor bulge formation [*Avicola and Huq*, 2003b].

[8] The theory of *Yankovsky and Chapman* [1997] assumes a steady state bulge, but both laboratory and numerical simulations suggest that bulges are unsteady features and that the volume of fluid in the recirculating bulge can continue to

grow over a long time scale in the absence of any remotely forced processes [*Avicola and Huq*, 2003a; *Fong and Geyer*, 2002; *Horner-Devine et al.*, 2006; *Nof and Pichevin*, 2001]. Hence, with a portion of the estuarine outflow going to bulge formation, freshwater transport in the coastal current is less than the river discharge. *Fong and Geyer* [2002] found that the fraction of river discharge transported by the coastal current decreases with increasing Rossby number, from 60% to 30% as the Rossby number increased from ~0.13 to ~3.7. In addition to outflow geometry, bulge formation and structure are modified by remotely forced shelf-wide circulation, winds, tides [*Fong and Geyer*, 2002; *Valle-Levinson et al.*, 1996; *Yankovsky and Chapman*, 1997; *Guo and Valle-Levinson*, 2007; *Choi and Wilkin*, 2007] and variations in river discharge [*Yankovsky et al.*, 2001].

[9] Tidal mixing in the estuary is a dominant process controlling outflow stratification [*Lerczak et al.*, 2006] and consequently plumes stratification. Numerical simulations of Chesapeake Bay by *Guo and Valle-Levinson* [2007] yields a bottom-advected plume when tides are included, while the plume becomes surface advected in simulations without tidal forcing. The spring/neap cycle in the Hudson River and the associated variations in mixing are well documented [*Chant et al.*, 2007; *Lerczak et al.*, 2006; *Peters*, 1997] and contribute to a fortnightly cycle in the buoyant discharge. While the fortnightly response of estuarine stratification is well known, less is documented about the corresponding plume response, although *Wong* [1998] notes variability in the Delaware River plume associated with spring-neap variability. Local tidal mixing in the near-field plume [*MacDonald et al.*, 2007; *Whitney and Garvine*, 2007] is a possible mechanism controlling plume stratification, although its importance relative to estuarine mixing is unknown. Moreover, wind mixing in the plume may obscure the spring/near-variability down coast.

[10] There are numerous studies of the wind forcing of river plumes that address steady wind regimes [*Choi and Wilkin*, 2007; *Fong and Geyer*, 2001; *Geyer et al.*, 2004; *Houghton et al.*, 2004; *Whitney and Garvine*, 2005] but rather few that consider highly variable forcing such as the sea/land breeze system (SLBS) [*Miller et al.*, 2003]. This despite the SLBS being a feature of coastal zone meteorology along many of the world's coastlines [*Gille et al.*, 2003; *Simpson*, 1994]. SLBS events are common along the coastline of New Jersey and Long Island [*Bowers*, 2004] during spring and summer. While most coastal studies of the sea breeze are focused on shelf waters [*Lerczak et al.*, 2001; *Simpson et al.*, 2002; *Hyder et al.*, 2002; *Hunter et al.*, 2007], we note that *Pinones et al.* [2005], in a study of the Maipo river in central Chile, found evidence of SLBS forcing of a river plume.

[11] The study presented here is motivated by observations made during the three field seasons of the Lagrangian Transport and Transformation Experiment (LaTTE) in 2004, 2005, and 2006, showing significant variability in the plumes structure at diurnal and fortnightly time periods. In particular, *Chant et al.* [2008] show evidence that the outflow trajectory alters with SLBS forcing, and this in turn may play a significant role in bulge formation and, ultimately, in the dispersal of the estuarine discharge across the shelf. These dispersal processes play a significant role in the evolution of physical, chemical, and biological properties of the Hudson River plume, the documentation of which is a primary objective of the LaTTE program. Here we focus on quantifying the effect that tides and SLBS forcing have on bulge formation and transport in the coastal current. We note that coastal currents and bulges represent two radically different transport pathways. In coastal currents, freshwater and material are rapidly transported down shelf, while bulge formation represents both cross-shelf transport pathway and also a mechanism to retain suspended material near the estuarine mouth. In this study we refer to the bulge region as a region of freshwater retention near the source of a buoyant outflow. This is more general than the commonly used definition of an anticyclonic eddy in cyclostrophic balance but appropriate due to the complicated nature of the dynamics involved.

[12] This article is organized as follows. Section 2 describes the study area and the observational data. Section 3 contains examples of observations showing spring/neap variability and SLBS forcing of the river plume. The Regional Ocean Modeling System (ROMS) configuration for this application is described in section 4, and the simulation results are presented in section 5. Section 6 summarizes the results and conclusions.

2. Study Area and Measurements

[13] The LaTTE study area extends from the south shore of Long Island, New York to Atlantic City, New Jersey and approximately 80 km offshore of Sandy Hook, New Jersey (Figure 1). Field efforts in May 2004, April 2005, and May 2006 include mooring deployments and shipboard surveys carried out within a sustained coastal ocean observatory. The observatory is designed, built, and operated by the Rutgers University Coastal Ocean Observation Lab (RUCOOL) and described in detail in the study of *Glenn and Schofield* [2004]. While there are myriad data sets available, the RUCOOL data sets used in this study include the Moderate Resolution Imaging Spectroradiometer (MODIS) chlorophyll *a* satellite data product as well as the Coastal Ocean Dynamic Applications Radar (CODAR) surface ocean current data. CODAR data used in this study is limited to the RUCOOL standard range system, which is limited in spatial extent to a region near the mouth of the Hudson River (Figure 1). The MODIS spatial coverage encompasses the entire LaTTE domain.

[14] Mooring data used here are from the inner shelf in 2005 and 2006. These include surface, middepth, and bottom salinity sensors as well as an Acoustic Doppler Current Profiler (ADCP) at each site. The moorings are located off Sandy Hook (N1), a three mooring line off of Belmar NJ (C1, C2, C3), and a southern mooring (S1) (Figure 1). Note that the C1–C3 mooring line changes from 2005 to 2006. Data archived by the National Data Buoy Center (NDBC) for stations at Sandy Hook (SDHN4) and Ambrose Light (ALSN6) are used for sea level and wind data, respectively. Discharge data for the Hudson River is provided by the USGS National Water Information System (http://waterdata.usgs.gov).

[15] In addition to the observational data, a modeling effort using the Regional Ocean Modeling System (ROMS) is a component of the LaTTE program [*Choi and Wilkin*, 2007; *Zhang et al.*, 2009a, 2009b]. We have adapted the model (section 4) in this study to consider and quantify the

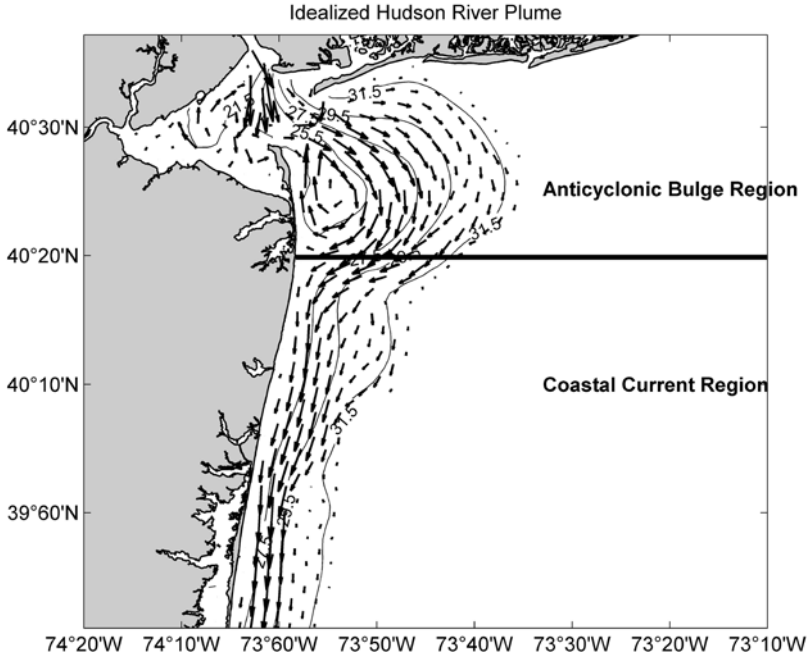

Figure 2. Idealized ROMS output showing the isohalines and current vectors of the surface signature of a surface-advected river plume.

impact of tides and SLBS forcing on the plume's transport pathways.

3. Observations

[16] The classic conceptual model (recirculating buldge and coastal current) of a surface-advected river plume is well established and illustrated in the idealized ROMS output (see section 4) in Figure 2. However, comparable field observations have proven somewhat elusive as this structure is often obscured by variability associated with tidal and wind forcing or remotely forced shelf-wide circulation, all of which can disrupt the pattern.

[17] Figure 3 depicts the surface signature of the plume using MODIS chlorophyll *a* images from an April climatology (Figure 3a) and snapshots from the 2004 (Figure 3b), 2005 (Figure 3c), and 2006 (Figure 3d) fields seasons. The climatology resembles the classic picture in Figure 2 with a clearly defined bulge and coastal current. There is, however, significant interannual variability. In 2004, during low river flow conditions, the plume also resembles the classic picture, with a bulge and coastal current (Figure 3b). A drifter deployed in the coastal current traveled southward at ~55 cm/s with the coastal current until the flow was arrested by upwelling winds. During the 2005 field study, which followed immediately after a near record river discharge [*Chant et al.*, 2008], the plume forms a large recirculating bulge with little or no coastal current (Figure 3c). Drifters deployed in 2005 move anticyclonically throughout the duration of the experiment, remaining in the bulge region. We note that during the 2005 field study, there is a strong and persistent SLBS and a near- zero mean wind [*Chant et al.*, 2008]. Oceanic conditions during the 2006 experiment were distinguished from both preceding years by the appearance of a relatively steady anticyclonic feature positioned downstream of the river outflow (Figure 3d). The narrow coastal current, evident in the drifter tracks, satellite imagery, and shipboard data (not shown), detached from the coast carrying flow offshore that subsequently recirculated back toward the coast. The drifters followed this offshore jet along the outside of the anticyclonic flow region (centered at approximately 40°N). The feature was not related to the low-salinity bulge that forms at the river mouth.

[18] Within each field season, the plume exhibits spring/neap variability in stratification as characterized by the surface-bottom salinity difference measured at the moorings (Figure 4). This effect is more evident in 2006 than in 2005 because the near record river discharge event in early April 2005 obscured the spring/neap variability of the outflow. However, during the second half of the 2005 record spring/neap variability in stratification is evident with increased stratification following neap tides on 3 and 17 May. In 2006 spring/neap variability in stratification is evident throughout the deployment with the strongest stratification following each neap tide at the beginning of May and June.

[19] The structure of the Hudson River outflow was also modified by diurnal forcing associated with the SLBS, particularly in 2005. Figure 5 illustrates the modification of the river outflow for two tidal cycles during an SLBS event in 2005. The offshore wind (toward the south) complements the ebb tide to drive the river outflow south (Figure 5a), presumably into the coastal current. The subsequent ebb (Figure 5c), responding to the onshore SLBS wind, is directed along the Long Island coast. This response is not limited to a single day. A time series of CODAR radial velocities (normal to the arc in Figure 1) over a 5 day period during the 2005 LaTTE experiment shows significant diurnal variability in the region of the river plume (Figure 6). The radial angles in Figure 6 are divided into 5° intervals of azimuth with respect to north, from 180° (southward) to 90° (eastward). Positive

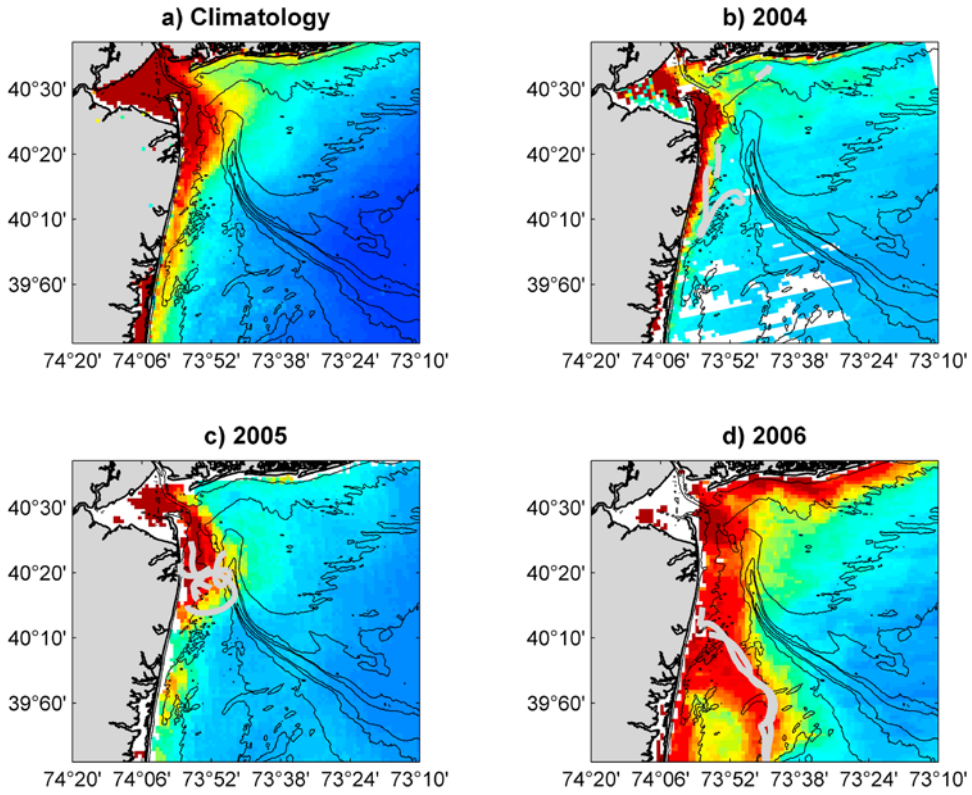

Figure 3. Moderate Resolution Imaging Spectroradiometer (MODIS) chlorophyll *a* images of the LaTTE study area for (a) April climatology (2004–2008), (b) 5 May 2004, (c) 4 April 2005, and (d) 28 April 2006. Higher chlorophyll concentrations (in red) are indicative of the presence of the Hudson River plume. Drifter deployments during the LaTTE experiments are shown in gray.

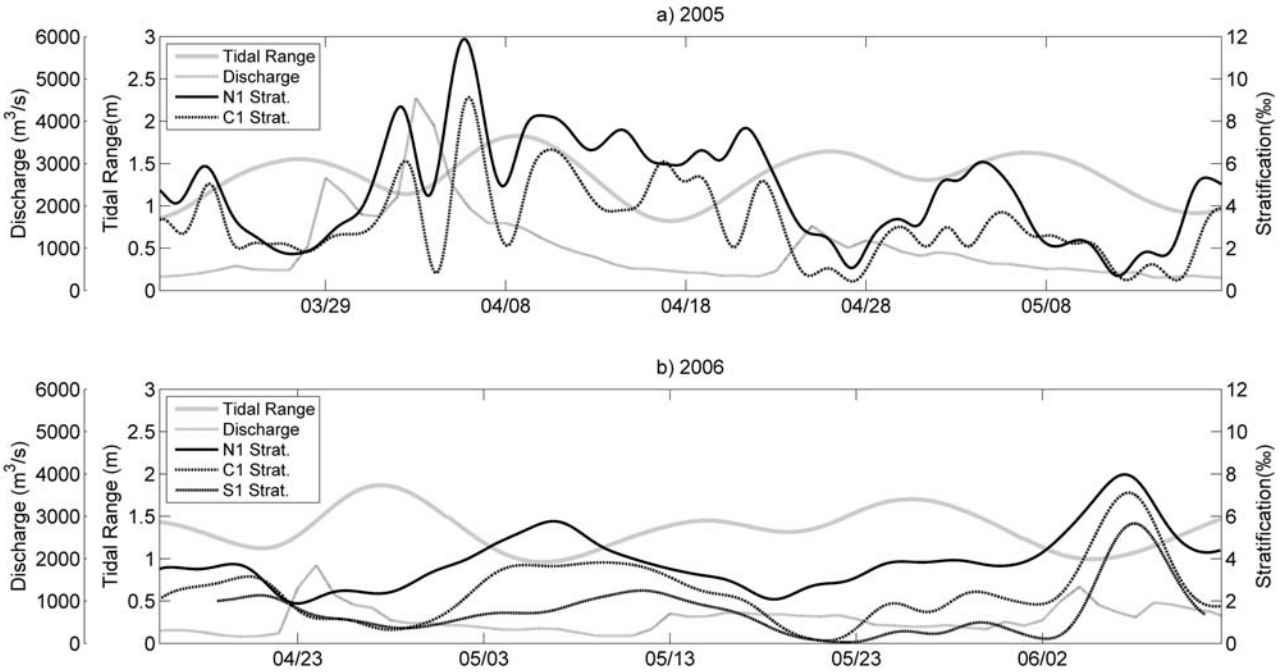

Figure 4. Time series of tidal range, stratification, and river discharge for the LaTTE mooring deployments in (a) 2005 and (b) 2006. Stratification is calculated as the top to bottom salinity difference at moorings N1, C1, and S1, low-pass filtered with a 72 h cutoff. The tidal range is the demodulated semidiurnal sea level at the Sandy Hook NDBC site.

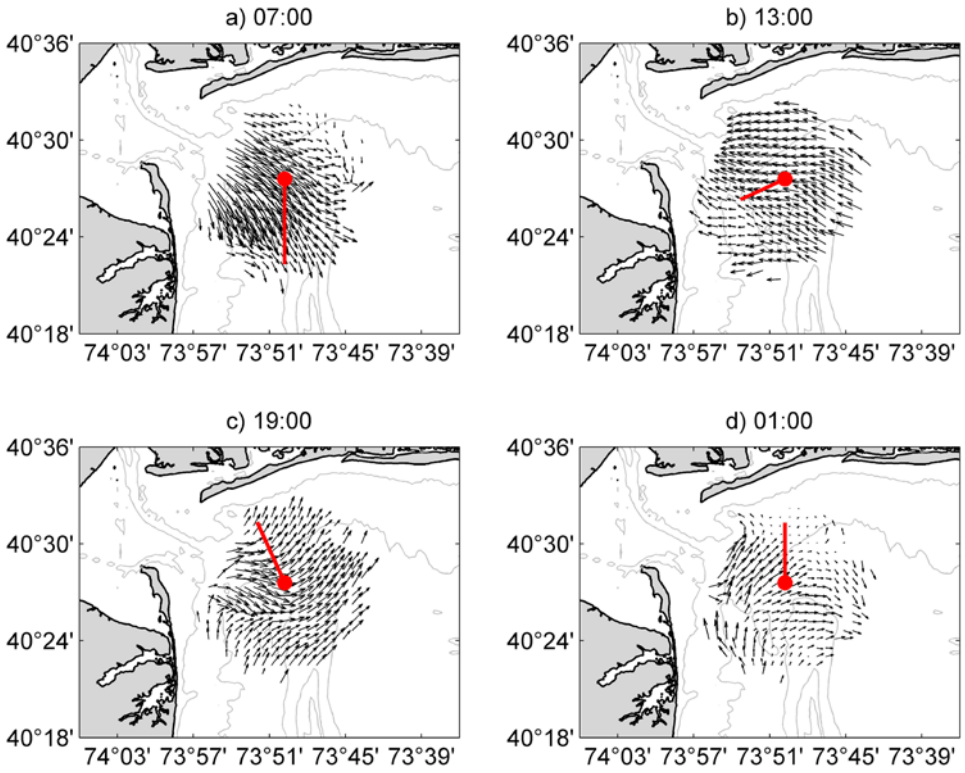

Figure 5. CODAR near-surface currents in 2005 showing (a) ebb tide with offshore wind, (b) flood tide during SLBS transition, (c) ebb tide with onshore sea breeze, and (d) end of ebb with onshore sea breeze.

values are directed away from the Hudson River mouth. Also shown on Figure 6 is the north-south component (positive to the north) of the wind at ALSN6, in which the SLBS manifests as a strong diurnal signal with a near-zero mean wind. During the nighttime, northerly wind phase of the SLBS radial velocities are positive in the southern part of the arc and negative in the north, indicating the current is to the west along Long Island and to the south along New Jersey. This phase of the SLBS should therefore favor coastal current formation. In contrast, during the afternoon southerly wind

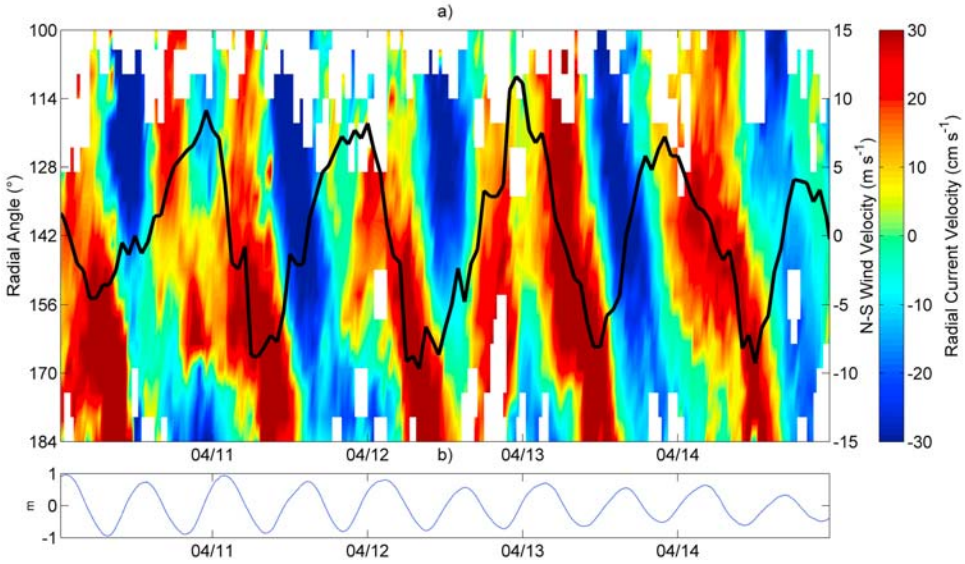

Figure 6. (a) CODAR radial velocity and north-south component (black line) of the wind (positive is to the north) at ALSN6. Radial velocity measurements are along the arc shown in Figure 1. 180° is south, and 90° is east. Positive values are away from the Hudson River mouth. (b) The water level at Sandy Hook (NDBC station SDHN4).

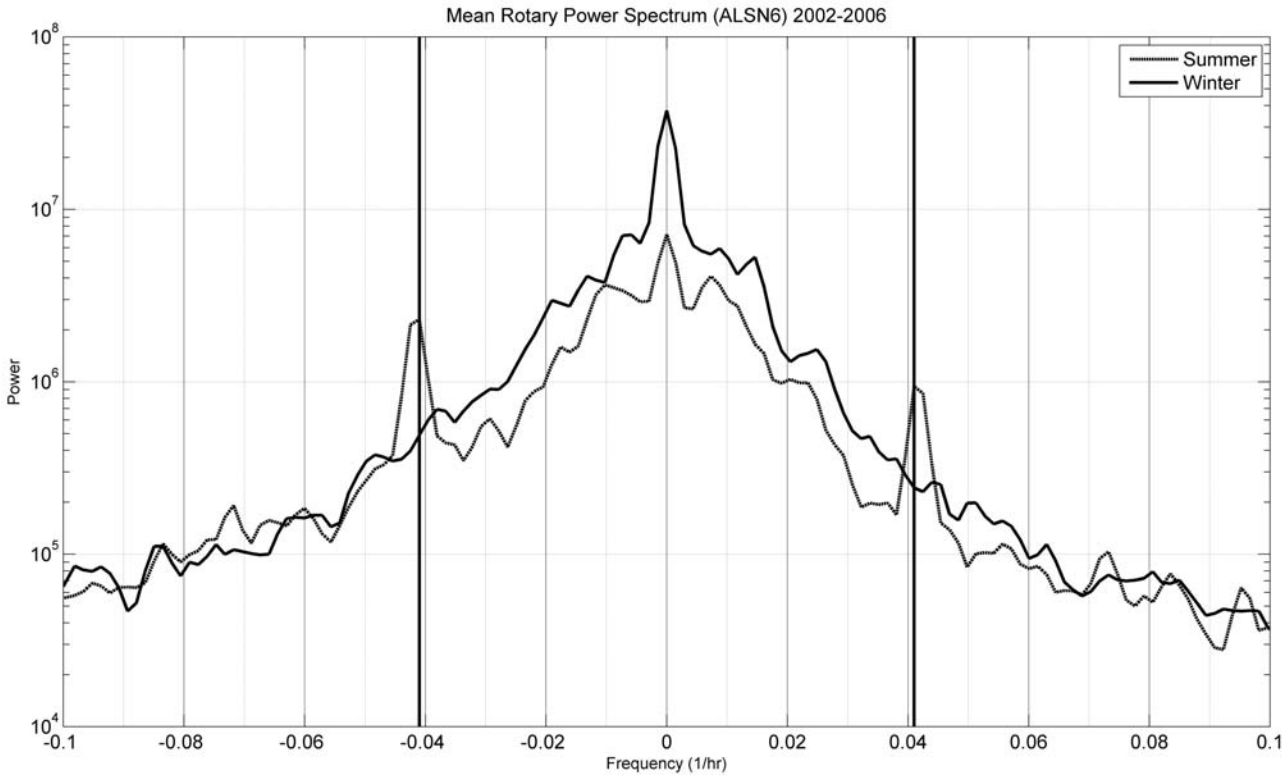

Figure 7. Mean rotary power spectrum of winds at ALSN6 for 2002–2006. The solid line is the winter spectrum, and the dashed line is the summer spectrum.

phase of the SLBS, the radial velocities are positive in the northern part of the arc and negative in the southern part; flow is to the north along New Jersey and to the east along Long Island. This phase of the SLBS directs freshwater away from the New Jersey coast and thus tends to reduce coastal current formation [*Chant et al.*, 2008].

[20] The SLBS is a well-known feature of New York/New Jersey coastal meteorology during the spring and summer months [*Hunter et al.*, 2007; *Pullen et al.*, 2007; *Colle et al.*, 2003]. Figure 7 shows the wind mean rotary power spectrum at ALSN6 for the winter and summer months from 2002 to 2006. There is a sharp increase in diurnal band energy in the summer consistent with the SLBS and accompanied by a decrease in subinertial energy. Individual SLBS days are identified using the method described in the study of *Furberg et al.* [2002]. A day is identified as an SLBS day if there is a sufficient land-sea temperature gradient, and there is an offshore wind in the morning, followed by an onshore wind for at least 2 h, followed by an offshore wind. The percentage of SLBS days for each month from 2002 to 2006 is calculated and shown in Figure 8. The SLBS activity picks up sharply in April, which coincides with the spring freshet. Indeed, during the freshet, diurnal winds associated with the SLBS occur approximately 50% of the time. The freshet leads to a highly stratified plume in the New York Bight apex at a time of increased SLBS activity. The coincidence of sea breeze activity and the spring freshet occurs because they are both driven by the same seasonal change in heating; the freshet by the melting of winter snows in upstate New York and the SLBS by developing land/sea thermal gradients that are most pronounced in early spring.

[21] During this time of higher stratification, increased occurrence of SLBS, and decreased mean/low frequency wind magnitude (Figures 7, 8), the diurnal energy in the coastal ocean increases. *Hunter et al.* [2007] documented increased diurnal energy due to the SLBS in the New York Bight apex during 2005. The kinetic energy of the diurnal wind at Ambrose increases (Figure 9) in April and remains high until September. Also in Figure 9 is the percentage of total kinetic energy in the diurnal band of the CODAR record for each month. The diurnal energy increases from ~1%–2% in the winter to 10%–15% in the summer. While 10%–15% is a modest increase, the SLBS events and the ocean response are episodic in nature. The increase in percentage of diurnal kinetic energy is due in large part to the absolute increase in diurnal energy of the surface current rather than a decrease in total kinetic energy. Wavelet transforms are presented in Figure 10 of the spatially averaged CODAR data and the ALSN6 wind data in 2007. While 2007 is not a LaTTE field year, it has the most complete record for winds and CODAR. The diurnal band power time series for the winds and CODAR show little variability or intensity in the winter months. Toward the end of March, the diurnal power increases and is highly variable in both the CODAR and wind records, suggesting times when the ocean diurnal energy is a significant percentage of the total energy. In fact, *Hunter et al.* [2007] identified time periods where the diurnal energy was as much as 50% of the total energy.

[22] In summary, observations show evidence of a subtidal response in plume stratification to fluctuations in tidal range over the spring/neap cycle. The observations also show diurnal energy in the coastal ocean responding to the

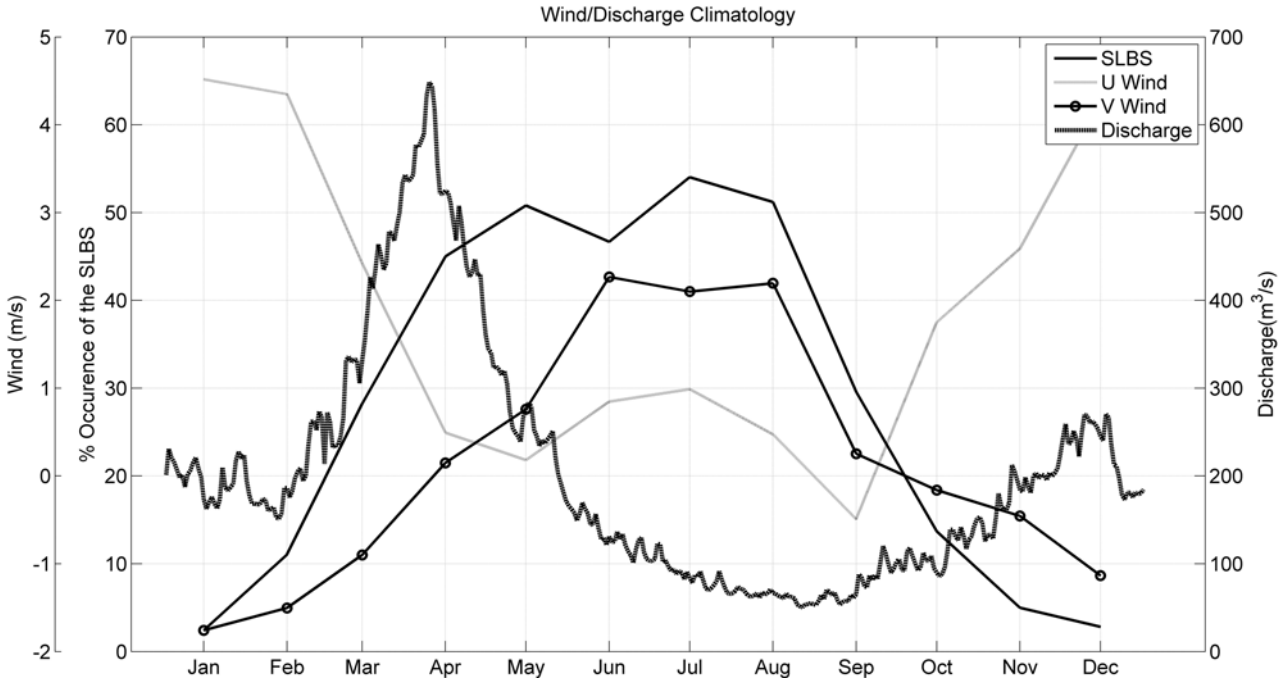

Figure 8. Climatology of Hudson River discharge, N-S (V) wind at ALSN6, E-W (U) wind at ALSN6 and SLBS occurrence [following *Furberg et al.*, 2002].

SLBS on seasonal and multiple-day time scales. It is further demonstrated that the diurnal energy in the region of the Hudson River plume represents a significant portion of the total kinetic energy. We suggest that the spring/neap variability could impact the dynamics of the plume by altering the Rossby and Froude numbers, which are set in part by stratification and are known to be important in determining many features of the plume [*Fong and Geyer*, 2002; *Horner-Devine et al.*, 2006; *Yankovsky and Chapman*, 1997]. We also suggest that the SLBS forcing may also

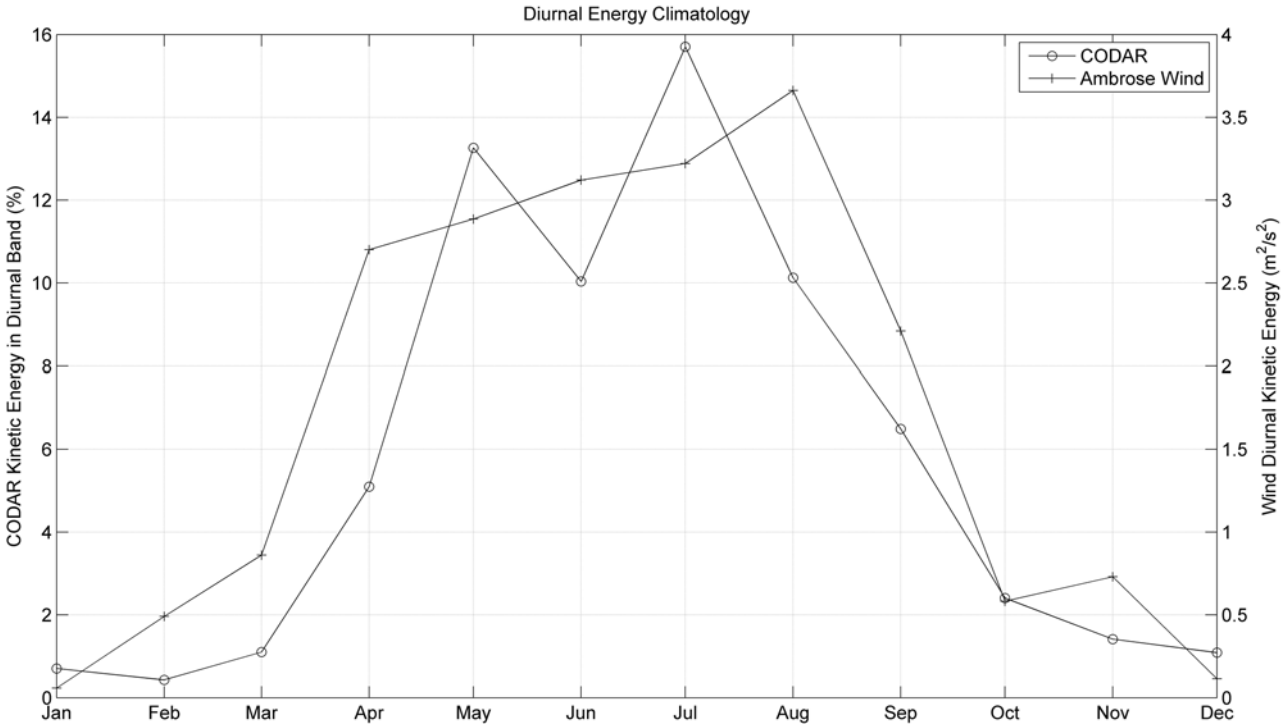

Figure 9. Climatology of the diurnal kinetic energy of the wind at ALSN6 (solid) and the percentage of total kinetic energy in the diurnal band (dashed) in the CODAR record for 2004–2007.

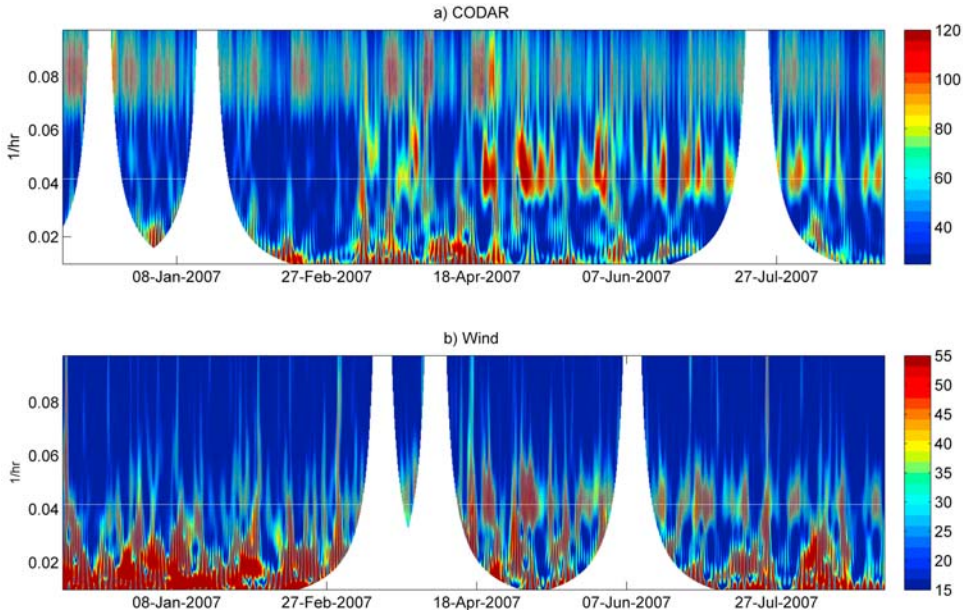

Figure 10. Time series of the magnitude of complex wavelet coefficients for (a) the CODAR surface current record and (b) the ALSN6 wind record. The diurnal frequency is the white dashed line.

play an important role by impacting the outflow angle, which it has been suggested plays a central role in bulge formation [*Avicola and Huq*, 2003b] and, subsequently, plume dispersion. To test these conjectures, we have conducted a set of ROMS model simulations to elucidate the effect of tides and diurnal wind variability on freshwater transport pathways.

4. Model Description

[23] The Regional Ocean Modeling System (ROMS; http://myroms.org) is a three-dimensional, free-surface, hydrostatic, split-explicit, primitive-equation ocean model that has been applied to numerous studies of regional ocean dynamics including estuaries, river plumes, and inner shelf circulation [*Hetland*, 2005; *MacCready and Geyer*, 2001; *Warner et al.*, 2005; *Wilkin*, 2006]. Details of the ROMS algorithms are described in the study of *Shchepetkin and McWilliams* [2005] and other model features have been summarized by *Haidvogel et al.* [2008].

[24] The model grid used here is identical to that used by *Choi and Wilkin* [2007]. The computational domain is rectangular, rotated from north/east to align approximately with the shelf break, and extends well beyond the region shown in Figure 1. The horizontal grid resolution is 1 km, and there are 30 levels in a vertically stretched terrain following coordinate system. Following *Choi and Wilkin* [2007], we apply the *Mellor and Yamada* [1982] level 2.5 vertical turbulence closure scheme, and at the open boundaries Orlanksi-type radiation conditions on three-dimensional variables (tracers and velocity) augmented with tidal harmonic variability in depth-averaged velocity and sea level. Unlike *Choi and Wilkin* [2007], the only atmospheric forcing variable here is an idealized wind stress, with no imposed air-sea heat fluxes. A constant Hudson River discharge of 500 $m^3\ s^{-1}$ is used in all model runs, which is approximately the annual mean discharge. Each model run is initialized with constant salinity of 32‰.

[25] The tidal forcing applied at the open boundaries uses harmonics from the ADCIRC model derived tidal constituent data base of *Mukai et al.* [2002]. Three sets of simulations were run that forced the model with a single tidal constituent at the M_2 tidal frequency to investigate the role of tidal amplitude on bulge formation. The first set forced the model with the ADCIRC model mean tidal range in the New York Bight (0.74 m), a second forced the model with an increased M_2 tidal range (amplitude 0.97 m), while the third applied a decreased M_2 tidal range (0.36 m). These three runs represent typical average, spring, and neap tidal range conditions. Simulations were also forced with the set of constituents (M_2, S_2, N_2, O_1, K_1, M_4, M_6) to model actual spring/neap variability.

[26] The SLBS is simulated by applying a spatially uniform diurnally varying wind stress derived from the wind record at ALSN6 during the LaTTE 2005 field experiment. Using harmonic analysis, the diurnal wind during this period was determined to be a clockwise rotary wind with a major axis of ~6 m s^{-1}. Wind stress was subsequently estimated using a quadratic drag law with a drag coefficient of $\sim 1.0 \times 10^{-3}$. The New York Bight apex has coastlines to the north and west, each of which has the potential to generate an SLBS front, and this is apparent in the variable orientation of the major diurnal wind ellipse at Ambrose and captured by high-resolution regional meteorological models [*Pullen et al.*, 2007; *Colle et al.*, 2003]. Therefore, two SLBS wind forcing cases were examined: one with the ellipse major axis in the north-south (NS) direction and a second case with the major axis in the east-west (EW) direction. In the following section, we focus on results for the NS case. Results for the EW case are similar unless otherwise noted.

[27] In total, we present seven model runs. The three tidal ranges (neap, average, and spring) are each run without wind stress and also with SLBS wind stress yielding six simula-

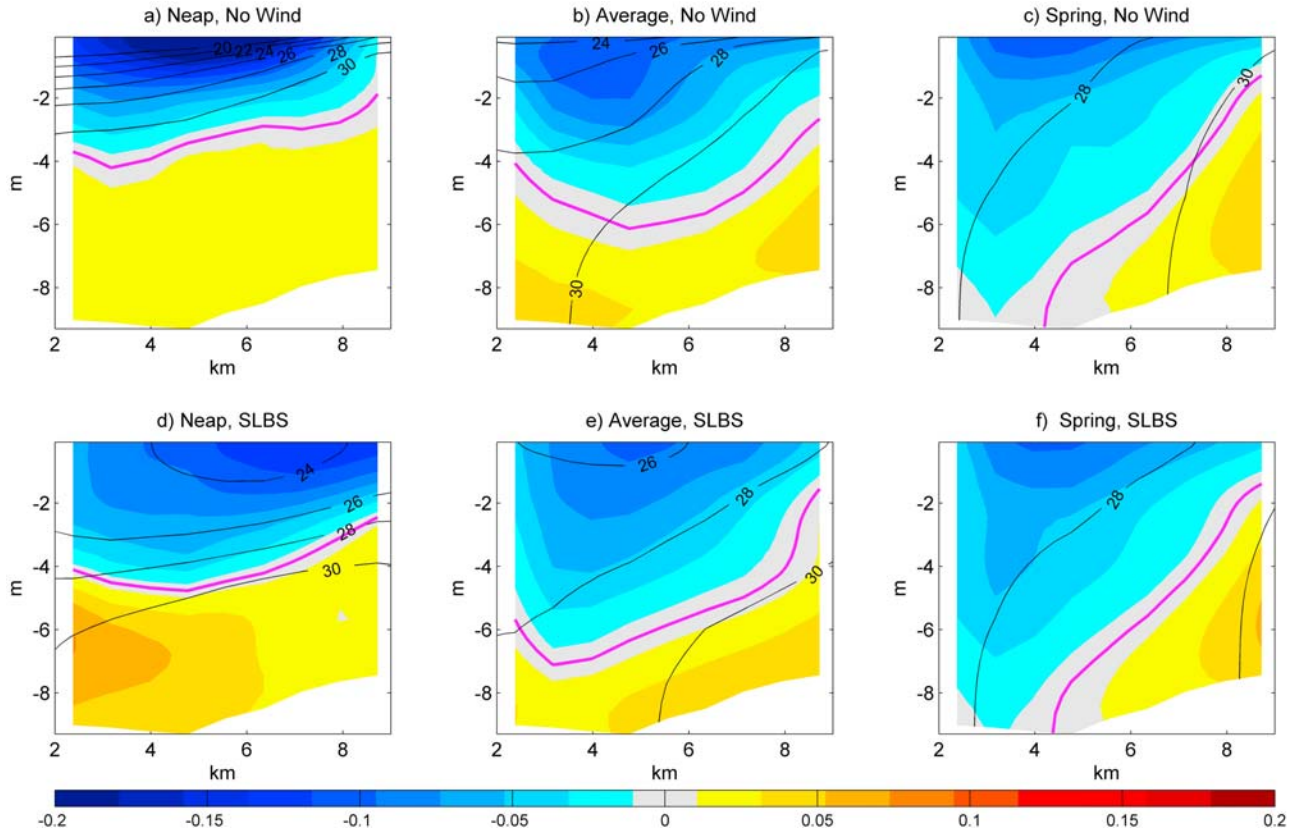

Figure 11. Cross section of the Hudson River outflow (transect A in Figure 1) with salinity contours (black) overlaid along channel velocity (m/s). Negative velocity is out of the estuary, and the zero velocity contour is shown in magenta. Model runs included are (a) neap tidal range/no wind, (b) average tidal range/no wind, (c) spring tidal range/no wind, (d) neap tidal range/SLBS, (e) average tidal range/SLBS, and (f) spring tidal range/SLBS.

tions. The seventh run was forced with the full complement of tidal constituents without wind to assess the time/scale of adjustment of the plume dynamics to fortnightly and monthly tidal variability. The results presented have been low-pass filtered so that we can assess the extent to which high-frequency forcing produces low-frequency response in the plume variability.

5. Model Results

[28] Each simulation was run for 60 days to allow freshwater transport in the coastal current to reach a quasi-steady, slowly varying state. (True steady state conditions were not a characteristic of any of the numerous studies of river plumes noted in section 1.) Figure 2 is an example of such a state, for the no wind, average tidal range case. The mean circulation in the model outside the plume region is negligible for all model runs presented in this study, suggesting little or no rectified flow through the interaction of tides, SLBS, bathymetry, and coastal shape.

[29] In order to characterize the nature of the surface-advected plume in a manner similar to the studies of *Avicola and Huq* [2003a, 2003b] and *Yankovsky and Chapman* [1997], we estimate outflow parameters for a section from Sandy Hook to Rockaway Point (line A in Figure 1). Figure 11 shows salinity contours and velocity normal (along channel) to this transect on model day 30. The greatest differences between the six cases are associated with varying tidal range and the variability over the spring/neap cycle is consistent with the mechanism described by *Lerczak et al.* [2006]. The neap tidal range/no-wind case (Figure 11a) has the thinnest, freshest outflow and is completely detached from the bottom. This case exhibits a fairly symmetric cross section with some cross-channel tilting of isohalines. The neap tidal range/NS SLBS case (Figure 11d) is similar, although mixing due to the diurnal winds has deepened the buoyant outflow by 1–2 m.

[30] The average tidal range model runs (Figures 11b and 11e) have a deeper halocline and outflow compared to the corresponding neap tide cases. For all tidal regimes, the surface salinity is lower for the no-wind case compared to the corresponding SLBS case. Increased tidal range is accompanied by increased tilting of isohalines and a developing asymmetry in the outflow with the center moving toward the Sandy Hook side of the channel. The spring tidal range case exhibits further deepening of the buoyant outflow layer (Figures 11c and 11f) and enhanced asymmetry across the section. The buoyant outflow intersects the bottom at the south side of the channel. The depth of the outflow is a critical parameter in defining the structure of the plume [*Yankovsky and Chapman*, 1997], and thus, we next look at its dependence on tidal and wind forcing.

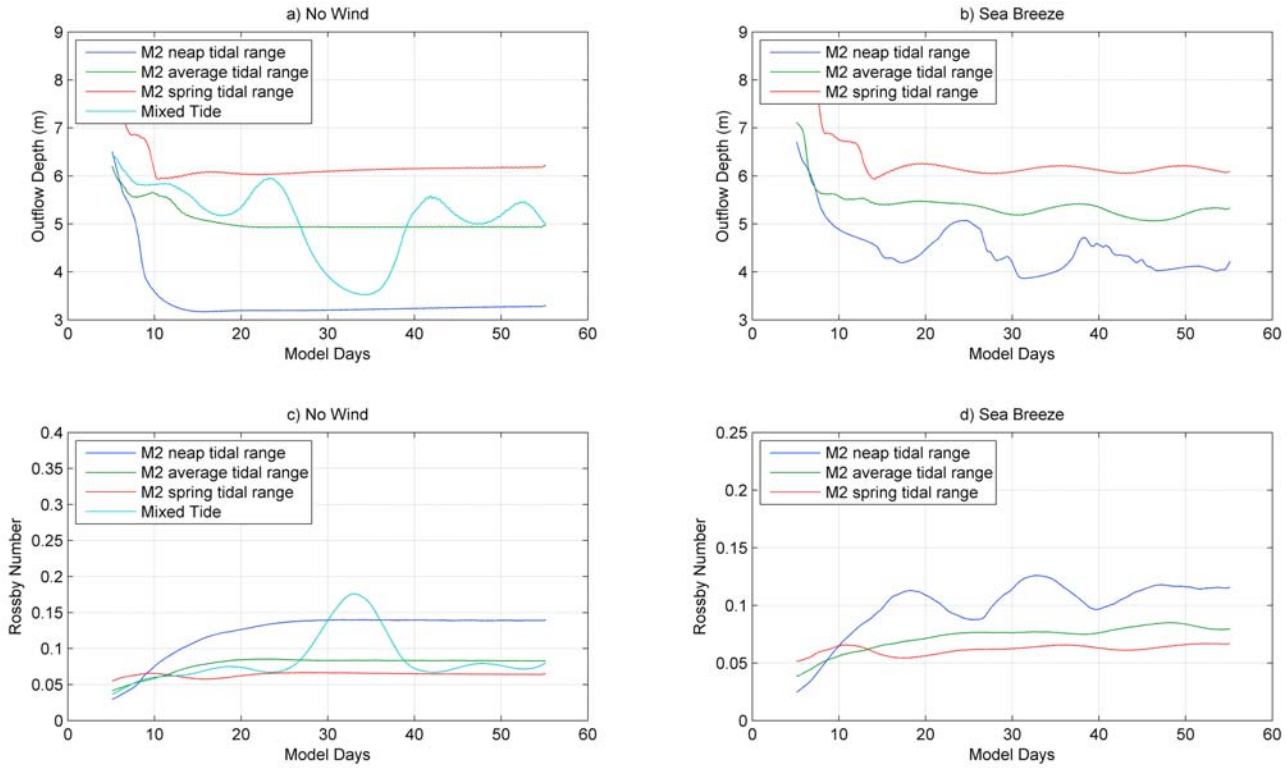

Figure 12. Time series of (a, b) outflow depth and (c, d) Rossby number for the Hudson River outflow calculated at transect A in Figure 1. (a) Outflow depth for the no-wind case. (b) Outflow depth for the SLBS case. (c) Rossby number for the no-wind case. (d) Rossby number for the SLBS case.

[31] We define the outflow depth h_o as the cross-channel average of the depth of the zero velocity isotach (magenta line in Figure 11) and plot the result in Figures 12a and 12b for each of the simulations. The outflow depth is generally stable throughout the model runs, equilibrating by about model day 10. The outflow depth in the average tidal range case is ~5.0 m for both wind regimes and ~6.1 m in the spring tidal range case, again for both wind regimes. In contrast, during the neap tide conditions, a thin (~3.3 m) outflow occurs in the absence of wind compared to ~4.2 m in the SLBS case. The outflow depth for the no-wind run with multiple tidal constituents modulates between 3.4 and 6.0 m from neap to spring tidal conditions, respectively, which is very close to the response to the idealized M_2 amplitudes we characterize as *neap* and *spring*. In summary, the outflow depth generally increases with increased tidal range with little variability due to wind regime except during times of decreased tidal range suggestive that wind mixing becomes less efficient as mixed layer depth increases.

[32] In a manner similar to *Yankovsky and Chapman* [1997], we use nondimensional Froude (1) and Rossby (2) numbers to characterize the buoyant plume. The outflow velocity (v_i) in (1) and (2) is defined as the mean velocity above the zero isotach and the width of the outflow (L) is 7 km. Reduced gravity in (1) is a layer reduced gravity, with the outflow density calculated as the mean density above the zero isotach. Variability in F_i and R_o across model runs is dominated by v_i, while variations in $(g'h_o)^{-1}$ are small by comparison. Time series of R_o are shown in Figures 12c and 12d. The relevant features of the F_i time series (not shown) are identical to that of R_o. Thus, variability that we ascribed to changes in the Rossby number may be dependent on the Froude number instead. Unfortunately given the constraints of the realistic grid, we were unable to separate Froude number dependence from Rossby number dependence in these runs. We note that for all model runs the magnitudes of F_i and R_o are similar, indicating buoyancy and Coriolis forces are comparable and suggesting a Burger number ($S = R_o/F_i$) near unity. The Burger number, a measure of the relative importance of stratification to rotation and is also the ratio of the inertial period (rotation) to the time scale associated with internal gravity wave propagating across the plume (stratification), maintains a magnitude from 0.6 to 0.75 for all cases.

[33] According to *Yankovsky and Chapman* [1997], a plume whose outflow satisfies the inequality $S > (2R_o)^{1/2}$ should be surface advected. Such a scaling is used to classify observed river plumes, despite the steady state nature of the theory. This condition is satisfied for all model runs in this study in agreement with previous modeling studies and shipboard observations during LaTTE, indicating the Hudson River plume is surface advected. There is also what appears to be a fortnightly variability (Figure 12d) in F_i and R_o in the decreased tidal range/SLBS model runs due to the beating between the diurnal SLBS and the semidiurnal tide.

[34] Cross sections of the coastal current are shown in Figure 13 corresponding to line B in Figure 1. Negative values are down shelf (in the Kelvin wave sense), and salinity contours are overlaid. Note that the salinity contour interval for Figures a13–13c is 1 ppt while for Figures 13d–

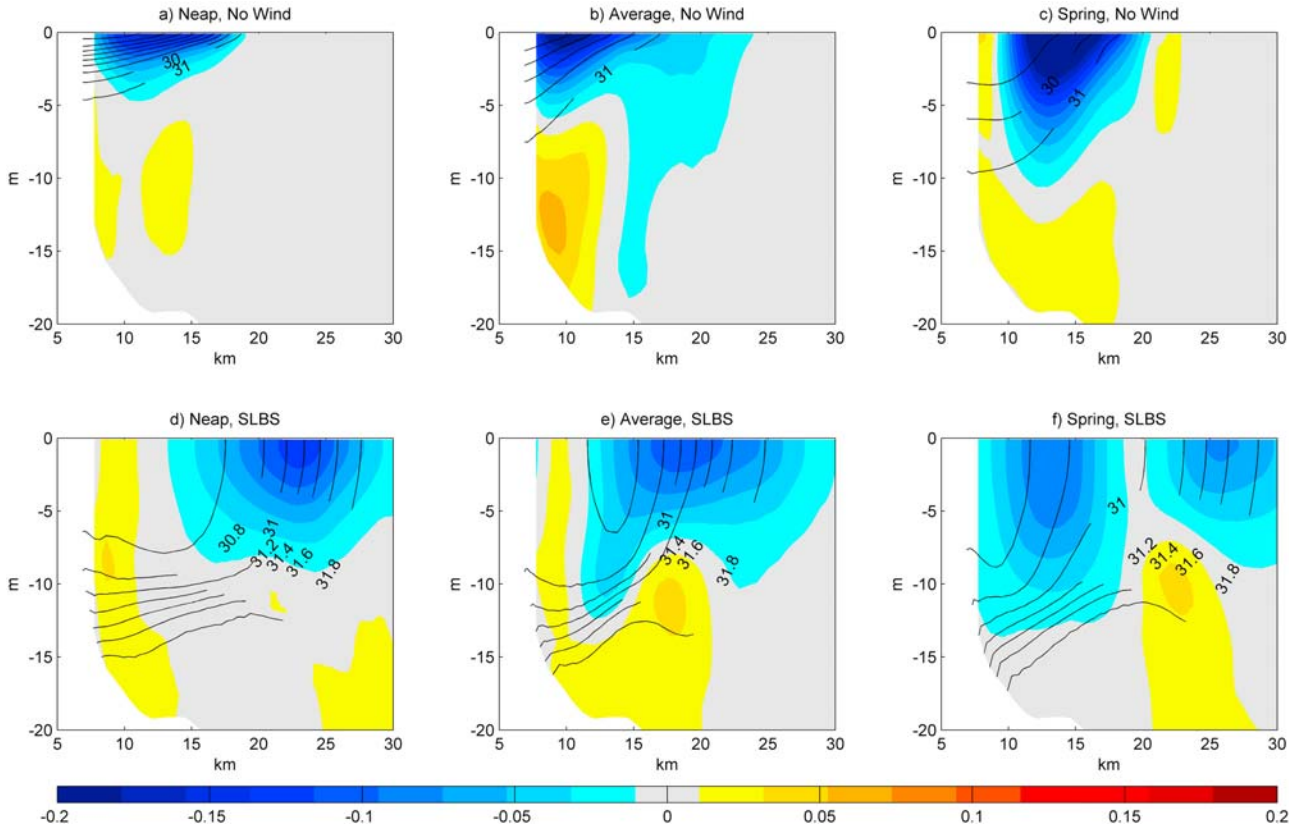

Figure 13. ROMS Salinity and current velocity (m/s) cross sections for transect B in Figure 1. Positive velocity is along shelf in the Kelvin wave sense (in blue). Please note the contour interval in Figures 13a–13c is 1 ppt and in Figures 13d–13f is 0.2 ppt. (a–c) The neap tidal range/no-wind, average tidal range/no-wind, and spring tidal range/no-wind cases, respectively. (d–f) The neap tidal range/SLBS, average tidal range/SLBS, and spring tidal range/SLBS cases, respectively.

13f is 0.2 ppt. Figures 13a–13c are the no-wind model runs for neap, average, and spring tidal ranges, respectively. As tidal range increases, stratification in the coastal current decreases and the depth of the coastal current increases. There is also little evidence of local tidal mixing in the plume when compared to the outflow cross sections in Figures 11a–11c. Figures 13d–13f show the corresponding SLBS results. Coastal current depths are similar for these three cases and much deeper (~10–15 m) than in the no-wind model runs. The deeper, wider halocline in these cases is evidence of enhanced local mixing due to the SLBS. The effect of spring/neap variability becomes less pronounced with wind forcing applied.

[35] Figures 14 shows time series of freshwater flux at line B expressed as a fraction of the river discharge (500 m^3 s^{-1}). Freshwater flux in the coastal current (Q_{cc}) is calculated as

$$Q_{cc} = \iint v \frac{s_o - s}{s_o} dA, \quad (4)$$

where v is along shelf velocity, s is salinity in the coastal current, s_o is the ambient shelf salinity (32‰), and A is the cross-sectional area.

[36] Figure 14a shows the no-wind cases. Low-pass filtered coastal current freshwater flux values are 0.5–0.9 of the river discharge for all cases, with the largest transport occurring for the spring tidal range. It is notable that for the spin-up period (~10–30 days) under neap tidal range conditions, the freshwater flux at line B increases much faster than in the average or spring tidal range cases. This corresponds to higher Rossby numbers and subsequently a tendency to favor bulge formation and a reduction of freshwater transport in the coastal current.

[37] Freshwater flux in the coastal current is further reduced by the introduction of SLBS forcing (Figure 14b), with the transport falling to approximately 1/2 of the river discharge for the case with spring tidal range and to less than 1/3 of river discharge for the neap tide case. While Figure 14b shows only the NS SLBS model runs, the freshwater flux in the EW SLBS model runs was even lower (~0.14–0.35 of river discharge). We note that while the SLBS forcing decreased the freshwater flux in the coastal current, the outflow Rossby number either decreased (neap tide case) or changed minimally (average or spring tide cases). This is in contrast to *Fong and Geyer*'s [2002] inverse relationship between Q_{cc} and R_o, suggesting that SLBS modification of the river outflow is less important than the plumes response to advective processes associated with SLBS. The SLBS forcing enhances bulge formation near the river mouth, thereby inhibiting freshwater transport in the coastal current.

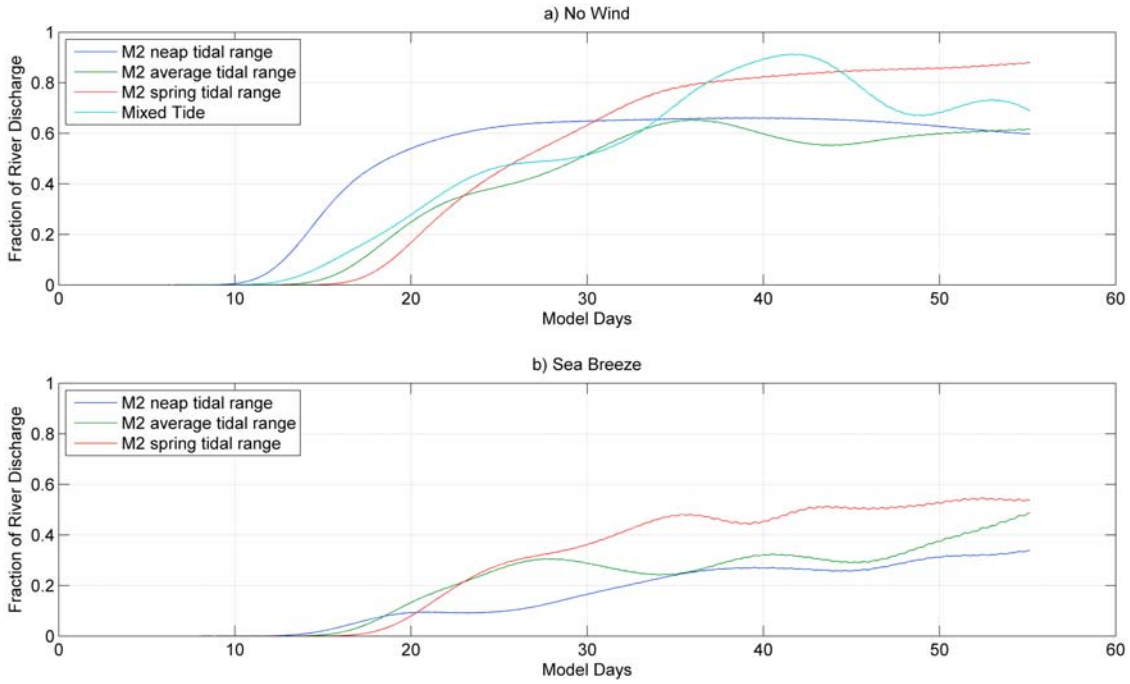

Figure 14. ROMS freshwater flux in the coastal current (transect B in Figure 1) for (a) the no-wind case and (b) the SLBS case. Flux values are expressed as a fraction of the constant river discharge of 500 $m^3 s^{-1}$. The SLBS wind forcing reduces freshwater flux in the coastal current by ~50%. The largest coastal current transport occurs during the strongest tidal range case for both the no-wind and SLBS regimes.

This accumulation of freshwater near the river mouth is due to the southerly phase of the SLBS that steers the outflow to the east and increases the outflow angle [*Chant et al.*, 2008], which favors bulge formation [*Avicola and Huq*, 2003b]. We note that in all tidal forcing cases the transport in the coastal current is decreased by 50% when sea breeze is added, which is consistent with the outflow being directed to the east and away from the New Jersey coast during the southerly phase of the SLBS. This scenario is also consistent with arguments by *Nof* [1988], who suggests that coastal current formation is inhibited when the recirculating bulge moves away from the coastal wall, which occurs 50% of the time when SLBS forcing is added. Thus, with SLBS forcing, we expect increased bulge formation which appears to be driven primarily by advective processes associated with the transport of freshwater to the east along Long Island's south shore.

[38] An example of the ocean response (average tidal range/SLBS model run) to the SLBS cycle during subsequent tidal cycles is shown in Figure 15. The result is similar to the CODAR example in Figure 5, i.e., subsequent ebbs interact with different phases of the SLBS. The first ebb (Figure 15a) during the offshore phase of the SLBS encourages transport into the coastal current, while the onshore phase of the SLBS forces the next ebb along the coast of Long Island. Over many SLBS cycles, the bulge region expands along the coast of Long Island, resulting in a net transport of freshwater to the east. Note, however, that in reality SLBS would be interrupted by cold fronts and storms that will radically modify the plume structure and potentially promote coastal current formation [*Choi and Wilkin*, 2007; *Zhang et al.*, 2009b].

[39] In order to illustrate the influence of SLBS on freshwater transport pathways, we calculate the equivalent depth of freshwater δ_{fw} [following *Choi and Wilkin*, 2007]

$$\delta_{fw} = \int_{-h}^{\eta} \frac{S_a - S(z)}{S_a} dz, \tag{5}$$

where S_a is the ambient shelf salinity (here $S_a = 32.0$), $S(z)$ is the salinity of the water column, η is the sea level, and h is the water depth.

[40] Examples of the development of the plume are shown in Figures 16a–16f. The outer edge of the plume is defined as the 0.25 m contour of δ_{fw}. Figures 16a–16c show the plume surface on model day 12 for decreased, normal, and increased tidal ranges, respectively. Figures 16d–16f is the same except for model day 40. The no-wind model runs are the solid contours, and the SLBS cases are the dashed contours. The plume structure is more responsive to SLBS forcing in the cases with neap tidal range when the plume is shallow and highly stratified. Under these conditions, the down-shelf penetration of the coastal current is significantly reduced and bulge formation significantly increased. Conversely, the response of the plume to SLBS forcing (relative to the no-wind case) becomes less pronounced as tidal range increases, although there is still a substantial decrease in freshwater transport. However, we note that during high-flow events, such as the 2005 freshet [*Chant et al.*, 2008], the plume can remain strongly stratified throughout the entire spring/neap cycle and be highly responsive to sea breeze forcing. Therefore, we suggest that SLBS forcing has a larger impact on freshwater dispersal during the spring freshet when discharge is high than during the summer months with low

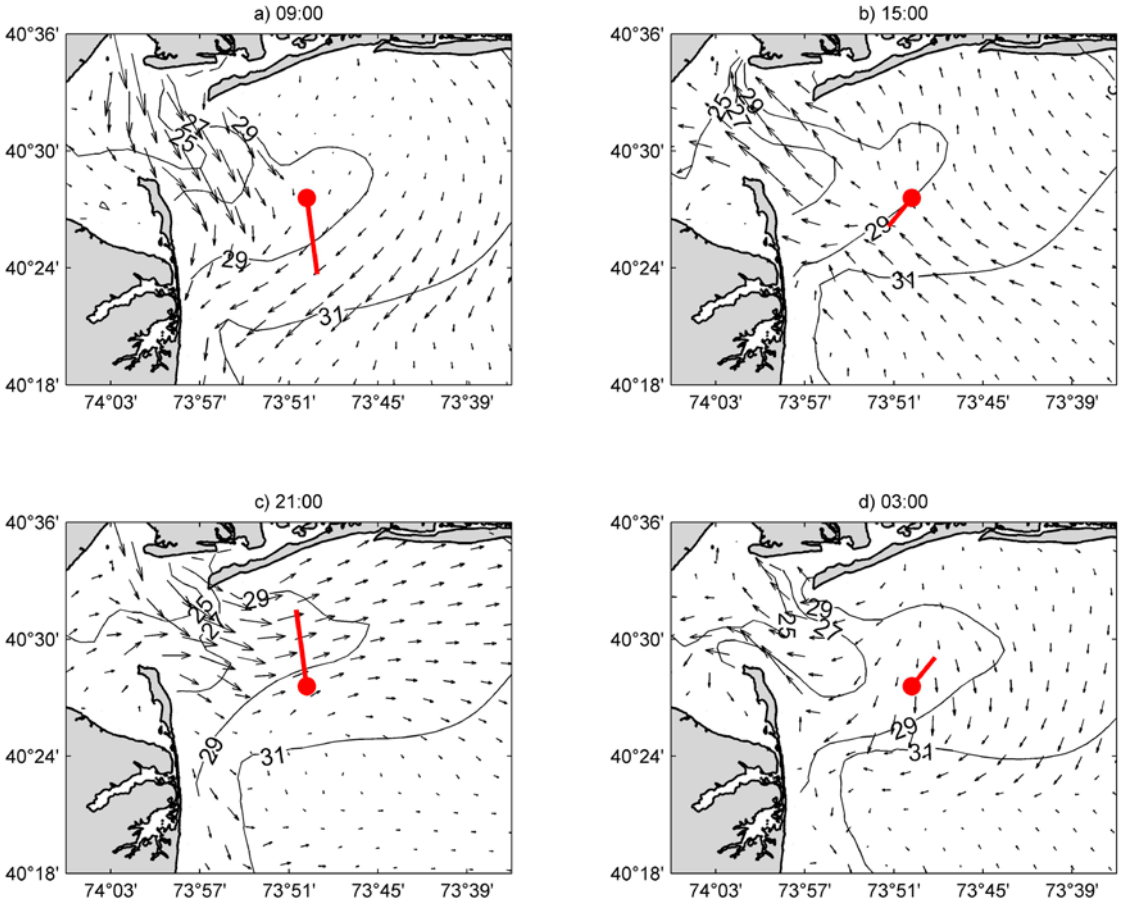

Figure 15. ROMS average tidal range/SLBS case showing near-surface currents for the (a) ebb tide with offshore wind, (b) flood tide during the SLBS transition, (c) ebb tide with onshore sea breeze, and (d) flood tide at the end of the SLBS cycle.

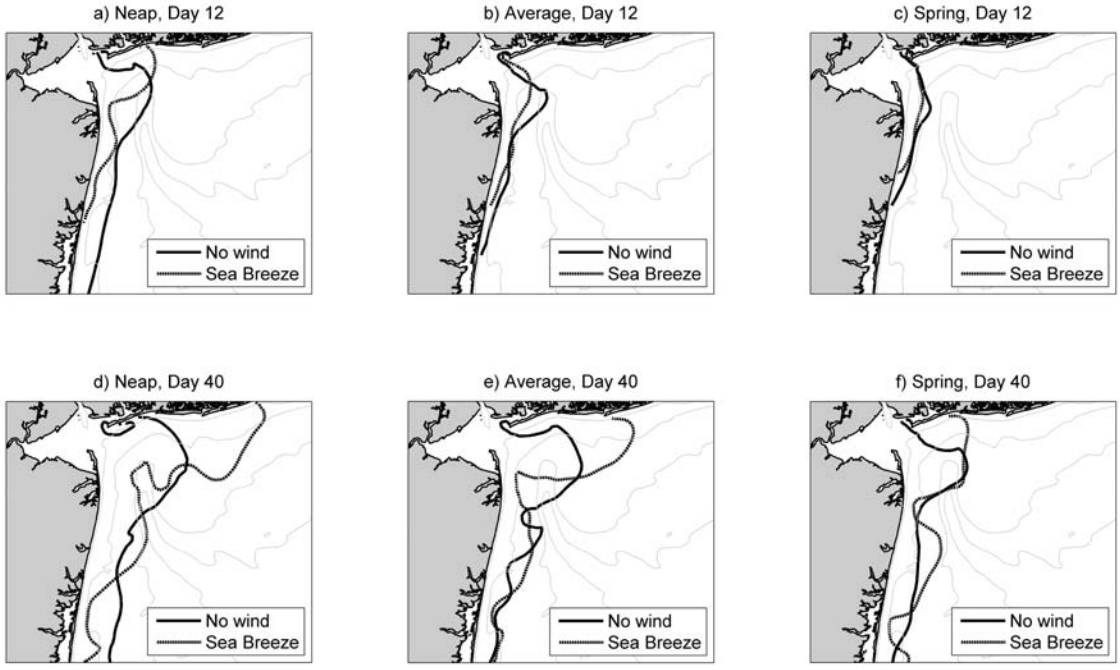

Figure 16. Equivalent depth of freshwater contour (0.25 m) for (top) day 12 and (bottom) day 40 for cases (a, d) neap tidal range, (b, e) average tidal range, and (d, f) spring tidal range.

discharge. More generally, these simulations indicate that the impact of SLBS forcing on river plumes diminishes with increased plume thickness.

[41] In Figure 16, there is also a notable transport of freshwater toward the east along Long Island during SLBS cases, contrary to accepted coastal current theory. This is particularly evident during the neap tidal range case, suggesting a net freshwater transport pathway assisted by variable winds in the New York Bight apex. Eventually the freshwater along Long Island's shore does turn south. These transport pathways, for simulations using observed winds and remote forcing, are discussed by *Zhang et al.* [2009a].

6. Summary

[42] Observations during the LaTTE 2004, 2005, and 2006 field seasons show that the structure of the Hudson River's outflow exhibits significant variability on a range of time scales. While much of this can be explained by variability in river discharge and the synoptic wind band, high-frequency forcing associated with tides and SLBS events also plays a significant role in shaping the structure of the plume. Stratification in the coastal current shows clear spring/neap tidal variability associated with variation in mixing within the Hudson River estuary as local tidal mixing in the plume is negligible. While the spring tide produces a less stratified coastal current, it also enhances coastal current transport. We suggest this latter result occurs for two reasons. First, while tidal currents are stronger during spring tide conditions the tidal mean velocities (i.e., that of the plume) are swifter during neap tides, and this increased horizontal advection increases the outflow Rossby number, which favors bulge formation, thus robbing the coastal current of transport [*Fong and Geyer*, 2002]. Second, during spring tides the spatial structure of the estuarine exchange flow becomes more laterally sheared with the outflow concentrated along the New Jersey coast, while during neap tides the exchange is more vertically sheared and the outflow is displaced from the coast. The spring tide lateral shear results in a river plume favoring coastal current formation, as evidenced by increased freshwater transport in the coastal current at these times. Conversely, during neap tides, the outflow is vertically sheared and more jet-like with the outflow swiftest away from the coast, which tends to favors bulge formation.

[43] The more significant result is that plume response to SLBS forcing is not only detectable but is a major mechanism determining the structure of the Hudson River plume during the spring and summer months. However, the outflow Rossby number argument, which fits the plume structure over the spring/neap cycle, is not consistent with the variation in coastal current for the SLBS results. The SLBS modifies the plume structure via a combination of advective and mixing processes outside the estuary, with advective processes seemingly dominating the transport pathways by sending 1/2 the outflow to the east along Long Island's south shore.

[44] This advective response is more pronounced when stratification is intensified during neap tides or when river discharge is high, i.e., there is a greater response to the SLBS in shallow, highly stratified plumes. The SLBS-dominated wind regime during the 2005 LaTTE field season coincided with a large recirculating bulge and limited freshwater transport in the coastal current. In particular, the phasing of the tides with respect to the SLBS is documented. CODAR radial velocities showed the outflow trajectory was strongly modified by SLBS forcing with the outflow directed to the east along the Long Island coast during the northward phase (sea breeze) of the SLBS and directed to the south along the New Jersey coast during the southward (land breeze) phase. We suggest that this essentially cuts the transport of the coastal current in half because the outflow during the northward phase is incorporated in the bulge. Numerical simulations suggest that the combination of neap tide conditions and SLBS winds reduces the transport of freshwater in the coastal current to less than 1/3 of the estuarine outflow, with the balance of the transport driving bulge formation. The resulting plume evolution provides a freshwater transport pathway along Long Island.

[45] The mixing response is clear in model cross sections of the coastal current. There is a deepening and vertical spreading of the halocline, coupled with the horizontal spreading of the plume. Although both mixing and advection are significant, we suggest that the plume's inviscid response to the SLBS plays the central role in reducing freshwater transport in the coastal current.

[46] Finally, SLBS conditions occur along many coastlines [*Gille et al.*, 2003] during spring and summer. It is likely then that coincidence of the spring freshet and SLBS activity is not unusual in temperate regions where the wintertime watershed stores precipitation as snowpack. Therefore, the results here suggesting that high-frequency variability and, in particular, the SLBS play a role in explaining lower-frequency variability in the Hudson River plume are likely to be echoed in other river plume systems globally.

[47] **Acknowledgments.** We thank the dedicated members of the Rutgers University Coastal Ocean Observing Lab, invaluable as sources of observatory data used in this study. We also thank Chip Haldeman for leading the mooring deployment and Gordon Zhang for providing support in the operation of ROMS. This study was supported by the National Science Foundation grant OCE-0238957.

References

Avicola, G., and P. Huq (2002), Scaling analysis for the interaction between a buoyant coastal current and the continental shelf: Experiments and observations, *J. Phys. Oceanogr.*, *32*(11), 3233–3248.

Avicola, G., and P. Huq (2003a), The characteristics of the recirculating bulge region in coastal buoyant outflows, *J. Mar. Res.*, *61*, 435.

Avicola, G., and P. Huq (2003b), The role of outflow geometry in the formation of the recirculating bulge region in coastal buoyant outflows, *J. Mar. Res.*, *61*, 411.

Bowers, L. A. (2004), The effect of sea surface temperature on sea breeze dynamics along the coast of New Jersey, M.S. thesis, 139 pp., Rutgers Univ., New Brunswick, N. J.

Castelao, R., O. Schofield, S. Glenn, R. Chant, and J. Kohut (2008), Cross-shelf transport of freshwater on the New Jersey shelf, *J. Geophys. Res.*, *113*, C07017, doi:10.1029/2007JC004241.

Chant, R. J., W. R. Geyer, R. Houghton, E. Hunter, and J. Lerczak (2007), Estuarine boundary layer mixing processes: Insights from dye experiments, *J. Phys. Oceanogr.*, *37*, 1859.

Chant, R. J., S. M. Glenn, E. Hunter, J. Kohut, R. F. Chen, R. W. Houghton, J. Bosch, and O. Schofield (2008), Bulge formation of a buoyant river outflow, *J. Geophys. Res.*, *113*, C01017, doi:10.1029/2007JC004100.

Chao, S.-Y., and W. C. Boiucourt (1986), Onset of estuarine plumes, *J. Phys. Oceanogr.*, *16*, 2137–2149.

Chapman, D. C., and S. J. Lentz (1994), Trapping of a coastal density front by the bottom boundary-layer, *J. Phys. Oceanogr.*, *24*, 1464–1479.

Choi, B.-J., and J. L. Wilkin (2007), The effect of wind on the dispersal of the Hudson River plume, *J. Phys. Oceanogr.*, *37*, 1878–1897.

Colle, B. A., J. B. Olson, and J. S. Tongue (2003), Multiseason verification of the MM5: Part I. Comparison with the eta model over the central and

eastern United States and impact of MM5 resolution, *Weather Forecasting*, *18*, 431–457.
Fong, D. A., and W. R. Geyer (2001), Response of a river plume during an upwelling favorable wind event, *J. Geophys. Res.*, *106*, 1067–1084, doi:10.1029/2000JC900134.
Fong, D. A., and W. R. Geyer (2002), The alongshore transport of freshwater in a surface-trapped river plume, *J. Phys. Oceanogr.*, *32*(3), 957.
Furberg, M., D. G. Steyn, and M. Baldi (2002), The climatology of sea breezes on Sardinia, *Int. J. Climatol.*, *22*(8), 917–932.
Garvine, R. W. (1995), A dynamical system for classifying buoyant coastal discharges, *Cont. Shelf Res.*, *15*, 1585–1596.
Garvine, R. W. (2001), The impact of model configuration in studies of buoyant coastal discharge, *J. Mar. Res.*, *59*, 193–225.
Geyer, W. R., R. P. Signell, D. A. Fong, J. Wang, D. M. Anderson, and B. A. Keafer (2004), The freshwater transport and dynamics of the western Maine coastal current, *Cont. Shelf Res.*, *24*, 1339.
Gille, S. T., S. G. Llewellyn Smith, and S. M. Lee (2003), Measuring the sea breeze from QuikSCAT Scatterometry, *Geophys. Res. Lett.*, *30*(3), 1114, doi:10.1029/2002GL016230.
Glenn, S. M., and O. Schofield (2004), Observing the oceans from the COOLroom: Our history, experience, and opinions, *Oceanography*, *16*.
Guo, X. Y., and A. Valle-Levinson (2007), Tidal effects on estuarine circulation and outflow plume in the Chesapeake Bay, *Cont. Shelf Res.*, *27*, 20–42.
Haidvogel, D. B., et al. (2008), Ocean forecasting in terrain-following coordinates: Formulation and skill assessment of the Regional Ocean Modeling System, *J. Comput. Phys.*, *227*(7), 3595–3624.
Hetland, R. D. (2005), Relating river plume structure to vertical mixing, *J. Phys. Oceanogr.*, *35*, 1667–1688.
Hickey, B. M., L. J. Pietrafesa, D. A. Jay, and W. C. Boicourt (1998), The Columbia River Plume Study: Subtidal variability in the velocity and salinity fields, *J. Geophys. Res.*, *103*(C5), 10,339–10,368, doi:10.1029/97JC03290.
Horner-Devine, A. R. (2008), The bulge circulation in the Columbia River plume, *Cont. Shelf Res.*, *29*, 234–251, doi:10.1016/j.csr.2007.12.012.
Horner-Devine, A. R., D. A. Fong, S. G. Monismith, and T. Maxworthy (2006), Laboratory experiments simulating a coastal river inflow, *J. Fluid Mech.*, *555*, 203–232.
Horner-Devine, A. R., D. A. Fong, and S. G. Monismith (2008), Evidence for the inherent unsteadiness of a river plume: Satellite observations of the Niagara River discharge, *Limnol. Oceanogr.*, *53*, 2731–2737.
Houghton, R. W., C. E. Tilburg, R. W. Garvine, and A. Fong (2004), Delaware River plume response to a strong upwelling-favorable wind event, *Geophys. Res. Lett.*, *31*, L07302, doi:10.1029/2003GL018988.
Hunter, E., R. Chant, L. Bowers, S. Glenn, and J. Kohut (2007), Spatial and temporal variability of diurnal wind forcing in the coastal ocean, *Geophys. Res. Lett.*, *34*, L03607, doi:10.1029/2006GL028945.
Hyder, P., J. H. Simpson, and S. Christopoulos (2002), Sea-breeze forced diurnal surface currents in the Thermaikos Gulf, north-west Aegean, *Cont. Shelf Res.*, *22*(4), 585–601.
Lentz, S. J., and K. R. Helfrich (2002), Buoyant gravity currents along a sloping bottom in a rotating fluid, *J. Fluid Mech.*, *464*, 251–278.
Lerczak, J. A., M. C. Hendershott, and C. D. Winant (2001), Observations and modeling of coastal internal waves driven by a diurnal sea breeze, *J. Geophys. Res.*, *106*, 19,715–19,729, doi:10.1029/2001JC000811.
Lerczak, J. A., W. R. Geyer, and R. J. Chant (2006), Mechanisms driving the time-dependent salt flux in a partially stratified estuary, *J. Phys. Oceanogr.*, *36*, 2296–2311.
Levinton, J. S., and J. R. Waldman, (2006), The Hudson River Estuary, Cambridge University Press, New York, 417 pp.
MacCready, P., and W. R. Geyer (2001), Estuarine salt flux through an isohaline surface, *J. Geophys. Res.-Oceans*, *106*, 11629–11637.
MacDonald, D. G., L. Goodman, and R. D. Hetland (2007), Turbulent dissipation in a near-field river plume: A comparison of control volume and microstructure observations with a numerical model, *J. Geophys. Res.*, *112*, C07026, doi:10.1029/2006JC004075.
Masse, A. K., and C. R. Murthy (1990), Observations of the Niagara River thermal plume (Lake Ontario, North America), *J. Geophys. Res.*, *95*(C9), 16,097–16,109.
Masse, A. K., and C. R. Murthy (1992), Analysis of the Niagara River Plume Dynamics, *J. Geophys. Res.*, *97*(C2), 2403–2420.
Mellor, G. L., and T. Yamada (1982), Development of a turbulence closure model for geophysical fluid applications, *Rev. Geophys. Space Phys.*, *20*, 851–875.
Miller, S. T. K., B. D. Keim, R. W. Talbot, and H. Mao (2003), Sea breeze: Structure, forecasting, and impacts, *Rev. Geophys.*, *41*(3), 1011, doi:10.1029/2003RG000124.
Mukai, A. Y., J. J. Westerink, R. A. Luettich, and D. J. Mark (2002), Eastcoast 2001, A tidal constituent data base for the western North Atlantic, Gulf of Mexico and Caribbean Sea. Engineer Research and Development Center/Coastal and Hydraulics Laboratory, *Tech. Rep. TR-02-24*, 196 pp.
Nof, D. (1988), Eddy-wall interactions, *J. Mar. Res.*, *46*, 527–555.
Nof, D., and T. Pichevin (2001), The ballooning of outflows, *J. Phys. Oceanogr.*, *31*, 3045–3058.
Orton, P. M., and D. A. Jay (2005), Observations at the tidal plume front of a high-volume river outflow, *Geophys. Res. Lett.*, *32*, L11605, doi:10.1029/2005GL022372.
Peters, H. (1997), Observations of stratified turbulent mixing in an estuary: Neap-to-spring variations during high river flow, *Estuar. Coast. Shelf S.*, *45*, 69–88.
Pinones, A., A. Valle-Levinson, D. A. Narvaez, C. A. Vargas, S. A. Navarrete, G. Yuras, and J. C. Castilla (2005), Wind-induced diurnal variability in river plume motion, *Estuar. Coast. Shelf S.*, *65*, 513–525.
Pullen, J., T. Holt, A.F. Blumberg, and R.D. Bornstein, (2007), Atmospheric response to local upwelling in the vicinity of New York–New Jersey harbor, *J. Appl. Meteorol. Climatol.*, *46*, 1031–1052.
Shchepetkin, A. F., and J. C. McWilliams (2005), The regional oceanic modeling system (ROMS): A split-explicit, free-surface, topography-following-coordinate oceanic model, *Ocean Model.*, *9*, 347–404.
Simpson, J. E. (1994), *Sea breeze and local winds*, Cambridge Univ. Press, Cambridge, New York, 234 pp.
Simpson, J. H., P. Hyder, T. P. Rippeth, and I. M. Lucas (2002), Forced oscillations near the critical latitude for diurnal-inertial resonance, *J. Phys. Oceanogr.*, *32*, 177–187.
Valle-Levinson, A., J. M. Klinck, and G. H. Wheless (1996), Inflows/outflows at the transition between a coastal plain estuary and the coastal ocean, *Cont. Shelf Res.*, *16*, 1819–1847.
Warner, J. C., W. R. Geyer, and J. A. Lerczak (2005), Numerical modeling of an estuary: A comprehensive skill assessment, *J. Geophys. Res.*, *110*, C05001, doi:10.1029/2004JC002691.
Whitney, M. M., and R. W. Garvine (2005), Wind influence on a coastal buoyant outflow, *J. Geophys. Res.*, *110*, C03014, doi:10.1029/2003JC002261.
Whitney, M. M., and R. W. Garvine (2007), Estimating tidal current amplitudes outside estuaries and characterizing the zone of estuarine tidal influence, *J. Continent. Res.*, *28*, 280–290.
Wilkin, J. L. (2006), The summertime heat budget and circulation of southeast New England shelf waters, *J. Phys. Oceanogr.*, *36*, 1997–2011.
Wong, K. C. (1998), On the variability in the vertical structure of the Delaware coastal current, *Cont. Shelf Res.*, *18*, 929–940.
Yankovsky, A. E., and D. C. Chapman (1997), A simple theory for the fate of buoyant coastal discharges, *J. Phys. Oceanogr.*, *27*, 1386–1401.
Yankovsky, A. E., B. M. Hickey, and A. K. Munchow (2001), Impact of variable inflow on the dynamics of a coastal buoyant plume, *J. Geophys. Res.-Oceans*, *106*, 19809–19824.
Zhang, W. G., J. L. Wilkin, and R. J. Chant (2009a), Modeling the pathways and mean dynamics of river plume dispersal in the New York Bight, *J. Phys. Oceanogr.*, *39*, 1167–1183.
Zhang, W. G., J. L. Wilkin, J. C. Levinand, and H. G. Arango (2009b), An adjoint sensitivity study of buoyancy- and wind-driven circulation on the New Jersey inner shelf, *J. Phys. Oceanogr.*, *39*, 1652–1668.

R. J. Chant, E. J. Hunter, J. Kohut, and J. L. Wilkin, Institute for Marine and Coastal Sciences, Rutgers, State University of New Jersey, New Brunswick, New Jersey 08901-8521, USA. (hunter@marine.rutgers.edu)